HIGH PRESSURE RINSING PARAMETERS MEASUREMENTS

E. Cavaliere, M. Fusetti, P. Michelato, C. Pagani, P. Pierini, R. Paulon, D. Sertore
INFN Milano – LASA, Via F.lli Cervi 201, I-20090 Segrate (MI), Italy

Abstract

High pressure rinsing with ultra pure water jet is an essential step in the high field superconducting cavity production process.

In this paper we illustrate the experimental characterization of a HPR system, in terms of specific power and energy deposition on the cavity surfaces and on the damage threshold for niobium.

These measurements are used to tentatively derive general rules for the optimization of the free process parameters (nozzle geometry, speeds and water pressure).

1 INTRODUCTION

High pressure rinsing (HPR) is nowadays routinely used in the process of superconducting RF cavities assembly to remove residuals from the resonator wall [1]. Despite the success of HPR in improving cavity performances, mainly reducing field emission, few studies have been performed to investigate the properties of the HPR jet at its impact on the superconducting cavities wall [2]. These are important issues for the future ILC (International Linear Collider) in order to improve performances and reliability of the HPR process for the cavities mass production. The purpose of this paper is to present the experimental set-up, the jet characterization and the path to the application of the results obtained in the optimization of the HPR process.

2 EXPERIMENTAL SETUP

The HPR system used for this experiment is based on an Ultra Pure Water system, a high pressure pump, a filter and a spray head with six nozzles.

Fig. 1 Load cell equipped with a 30° wedge for angular dependence measurement of water jet force and profile.

The high purity water ($\rho \geq 18$ MΩ·cm), generated from a SuperQ Millipore plant, is fed to a high pressure pump (Kärcher HD 600 C) able to supply 10 liters per minute at 100 bar. The high pressure water is filtered by a 40 nm-100 bar filter and then sprayed by a head mounting 6 nozzles. Each nozzle is 0.55 mm in diameter (Spraying System VS120) with a sapphire diaphragm.

A load cell TEDEA HUNTLEIGH mod. 505H-2M-2 (max load 2kg, resolution 1 g), placed at proper distances from the nozzle, characterizes the force exerted by the water jet. Moreover wedges are installed on the load cell as shown in Fig. 1 to measure the angular dependence of water force and profile as will be described below.

The Nb samples, used to simulate the cavity wall, were machined out of a RRR = 300 sheet and cleaned either with a 1:1:2 BCP solution for 1 min or $HF:HNO_3:H_2SO_4$ for 30 seconds.

2 JET FORCE AND PROFILE

The first step in the characterization of the 100 bar water jet is the determination of its total force and the its profile at different distances from the nozzle. Fig. 2 shows a typical scan of the jet impinging normally to the load cell. The water jet moves on the load cell from the top to the bottom with a vertical speed of 2.2 mm/min. From Bernoulli's law the expected force is 3.9 N, if no friction is assumed. The measured force value is of 3.5 N and hence the flow loss factor for our nozzle is 0.9 [3].

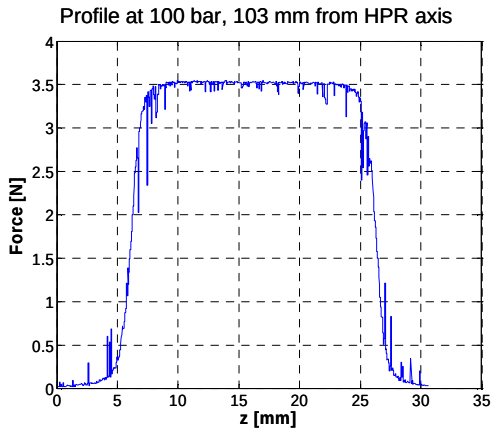

Fig. 2 Scan of the water jet profile on the load cell.

Moreover approximating the jet radial dependence with a Gaussian profile, Fig.2 allows to measure the jet spot dimensions applying

$$F(z) = \frac{F_0}{2} \cdot \left[1 + Erf\left(\frac{z - z_0}{\sqrt{2} \cdot \sigma} \right) \right]$$

at the rising and falling edge of the scan. F_0 is the total force and σ is the spot size. The jet parameters are calculated fitting $F(z)$ to the experimental values.

Measurements of the force profile at different distances from the nozzle (Fig. 3) results in a parameterization of σ versus distance r as

$$\sigma(r) = 0.0065 \cdot r + 0.1158$$

where all dimension are millimeter.

Consequently, the 190 Watt mean power of each of our jet corresponds, in the Gaussian approximation, to a peak power density of 250 Watt/mm^2 at 35 mm from the head axis.

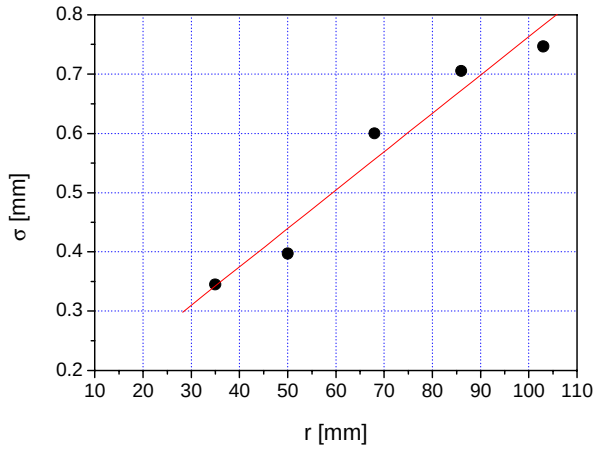

Fig. 3. Spot size evolution with respect to the radial position from the head axis. The nozzle exit is at 17.5 mm from the head axis.

We have also measured a linear dependence of force and spot size from the water jet pressure.

3 JET FORCE AND PROFILE ANGULAR DEPENDENCE

A further step in the water jet characterization is the measurement of the force and spot size versus the incidence angle on the sample.

This is important for the HPR parameter optimization especially for low beta cavities where the cavity wall is near to be perpendicular to the cavity axis. In this case, variation of force and spot size are significant and have to be taken into account.

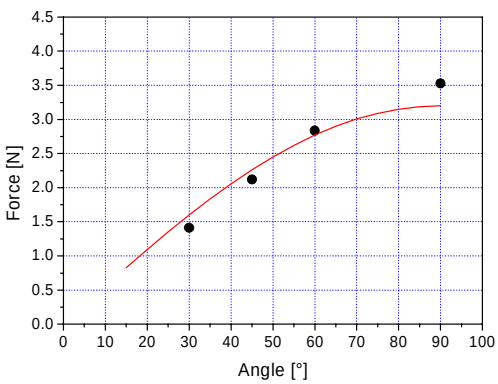

Fig. 4. Force angular dependence at 68 mm from the spraying head axis @ 100 bar.

To study the dependence of force and spot size from impact angle, we have mounted wedges with different apex angles (30°, 45° and 60°) on the load cell.

Fig. 4 shows the total force versus apex angle at 68 mm from the spraying head axis. A sine dependence, shown by the red line, is expected from momentum conservation. Similar results have been obtained at different distances from the head axis.

The spot size is also proportional to the reciprocal of the sine function as geometrical consideration suggests.

4 WATER JET STRUCTURE

One of the key points in the modeling of the cleaning process by HPR is the knowledge of the structure of the water jet to distinguish different mechanisms that contribute to the final results. In literature [4], it is reported that at the exit of the nozzle the water jet evolves from an hard core structure to a fully atomized water spray after a transition region where the hard core coexists with drops and bubbles of different dimensions.

During jet characterization, we imaged the jet using the induced luminescence visible on Plexiglas and glass targets. We observed a clear and reproducible annular structure on samples placed at 35 mm from the axis. The structure was not observable at larger distances as shown in Fig. 5.

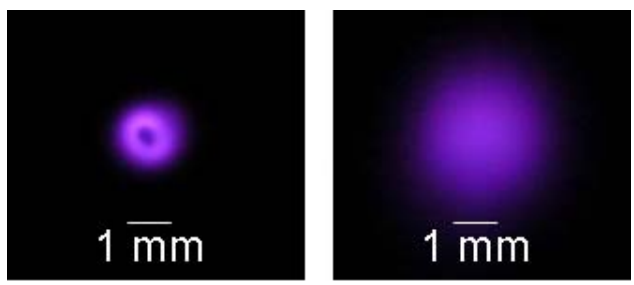

Fig. 5 Luminescence images of the high pressure water jet impinging on a Plexiglas screen placed at 35 mm (left) and 200 mm (right). An annular structure is visible on the 35 mm image but not on the 200 mm one.

The structured image visible at 35 mm is interpreted as an hard core jet near to its stagnation point (black central part) and luminescent ring outside. The hard core part of the jet vanishes at large distances. Moreover, the color depends on the environmental gas composition.

5 JET INDUCED NIOBIUM COLOR CHANGES

During the characterization of the HPR jet, we have also observed the appearance of colored ring at the interaction region of the water jet on Nb samples. The number and color of the rings depend, at fixed HPR parameters, from the exposition time of the sample to the water jet. Fig. 6 shows a typical color change of the Nb sample during exposition to the HPR water jet at 35 mm. As in the case of the luminescence images, also in this case the footprint at 35 mm has an annular shape with a central region less influenced than the outer ring. The

shape changes to a round form moving towards 103 mm position.

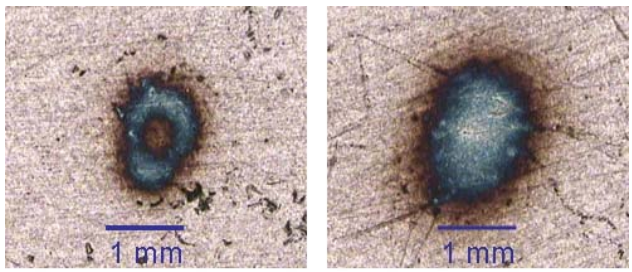

Fig. 6. Different shapes of the water jet effect on Nb samples. Left image was taken at 35 mm from the head axis, right one at 103 mm. The annular footprint disappear at longer distance.

The appearance of color rings was studied in the past and it was interpreted as an oxidation of the Nb sample under jet exposition [5]. We have performed XPS analysis on "103 mm" colored samples that revealed that, moving from the border to the center of the spot, the oxygen content indeed increase as well as Nb^{+5} while pure Nb signal decreased, indicating the formation of Nb_2O_5 oxide. From this analysis, we observed also a reduction of the fluorine signal present on the unwashed Nb sample (see Fig. 7).

The formation of a niobium oxide suggests that the colors are due to the interference fringes produced by the growth of the very thin oxide layer on the Nb surface, starting from the center and developing outwards.

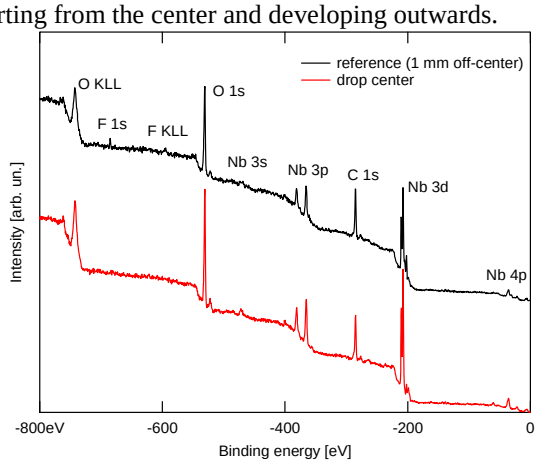

Fig. 7. XPS spectrum at the center of the of the sample (red line) and 1 mm off (black line).

The pattern similarity in the luminescence and oxidation pictures suggests a common origin of the phenomena. During our experiments, we observed formation of ozone, electrostatic charging of Nb samples ($i \approx 12$ μA) and luminescence effects visible only on dielectrics targets. Possible explanation are either electrostatic corona discharging or hydrodynamic cavitation of gas or vapor bubbles entrained in water jet that might produce both luminescence and oxidation, via production of chemical reacting species [6]. Further investigation are however needed in order to clarify the phenomena involved.

6 PATH TOWARDS PROCESS OPTIMIZATION

The optimization of the cleaning process requires an improvement and maximization of the cleaning capability of the jet and a deeper understanding of its mechanisms.

The water jet properties measured so far already allow to calculate patterns described by the jets on a cavity wall and some relevant physical quantities. For examples assuming a spot area equal to a circle of radius σ, Fig. 8 shows the static water jet pressure variation along the z axis for a TESLA cavity [7]. As expected the highest water pressure is at the iris while the minimum is on the wall near the equator and not on the equator itself due to the geometrical effect discussed before.

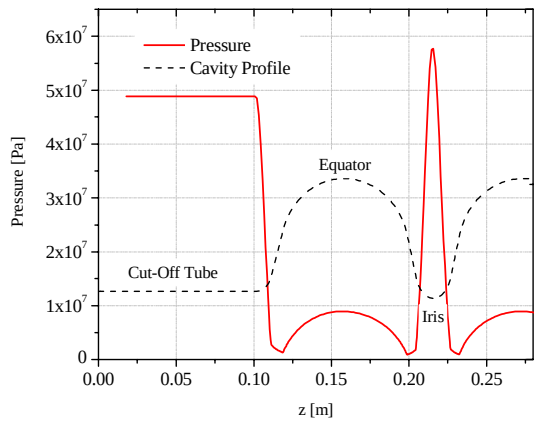

Fig. 8. Static water pressure variation on the cavity wall along the axis for a TESLA cavity using the jet dependences discussed before.

This is only a first step in the modeling. We are now considering the influence of the number of jets, nozzle angles, etc. on the cavity area covered by the jet itself.

CONCLUSION

We have started the characterization of an HPR system in view of the optimization of the cleaning process and some "geometrical" considerations are already possible. The optimization of the overall cleaning process needs a deeper understanding of the governing mechanisms.

7 ACKNOWLEDGMENT

We would like to thank A. di Bona of the INFM Modena - SESAMO laboratory for the XPS analysis.

8 REFERENCES

[1] P. Kneisel and B. Lewis, Part. Accel. 53 (1996), 97.
[2] R. Gim et al., 4th Symp. On Particle on Surf., p. 379.
[3] R. Reitz, "Fluid Mechanics", CRC Press LLC, 1999.
[4] C. Zou et al., 3rd US Water Jet Conf., USA, 1985.
[5] J. Knoblock et al.,Cornell SRF Note-980223-01, 1998.
[6] K. Suslick et al., J. Am. Chem. Soc. 119 (1997), 9303.
[7] B. Aune et al., PRSTAB 3, 092001 (2000).